Hydrodynamic interactions between pairs of capsules and drops in a simple shear: Effects of viscosity ratio and heterogeneous collision

Rajesh Kumar Singh and Kausik Sarkar

Phys. Rev. E **92**, 063029 — Published 29 December 2015

DOI: 10.1103/PhysRevE.92.063029

Hydrodynamic interactions between a pair of capsules in a simple shear: effects of viscosity ratio, heterogeneous collision and comparison with drops

Rajesh Kumar Singh[1,2] and Kausik Sarkar[1,2,3]

[1]Department of Mechanical Engineering
[2]Biomechanics and Movement Science Program
University of Delaware, Newark, DE-19716
[3]Department of Mechanical and Aerospace Engineering
The George Washington University, DC-20052
Email: sarkar@gwu.edu

Abstract

Hydrodynamic interactions between a pair of capsules in simple shear are numerically investigated using a front tracking finite difference method. Membrane of the capsule is modeled using different hyperelastic constitutive relations. We also compare the pair interactions between drops with those between capsules. Increased viscosity ratio leads to a reduced net cross-stream separation between capsules as well as drops after collision. At low viscosity ratios, drop-pairs show higher cross-stream separation than those for capsule-pairs, while substantially large viscosity ratios result in almost the same value for both cases. We investigate pair-collisions between two heterogeneous capsules C_1 and C_2 with two different capillary numbers. The maximum deformation of C_1 was seen to increase with increasing stiffness (decreasing capillary number) of C_2, even though the stiffness of C_1 was kept fixed. The findings are similar for a drop-pair, however with a smaller maximum deformation for the same combinations of capillary numbers. The final cross-stream drift of the trajectory of C_1 decreases with increasing stiffness of C_2, but the relative trajectory between the capsules remains unchanged. The maximum deformation and the cross-stream drift of trajectory of C_1 are shown to approximately vary with power-law functions of the ratio of the capillary numbers of C_1 and C_2. An analytical explanation of the dependence on the two capillary numbers is offered. Different membrane constitutive laws result in similar deformation and drift in trajectory.

I. Introduction

Blood is a suspension of different types of cell—erythrocytes, leukocytes and platelets—dispersed in plasma. They differ in size and physical properties such as membrane stiffness and viscosity; leukocytes are less deformable than platelets and erythrocytes. Deformability of cells affects their interactions and the overall effective rheology, which in turn impact physiological functions [1]. Many cardiovascular diseases arise from change in cell deformability and shape. For example, red blood cells (RBC) become stiffer in sickle cell anemia and malaria [2] restricting their passage through small arteries leading to reduced oxygen supply. Cells are complex objects consisting of internal organelles bounded by a lipid bilayer. Fluid capsules enclosed by an elastic membrane have become a useful model system for cells. Dynamics of a single capsule has been studied quite extensively 1[3-6]. In this paper, we investigate the interactions between a pair of capsules in free shear varying their deformability. Specifically, we study the effects of viscosity ratio and heterogeneity—two capsules having different membrane stiffness.

Hydrodynamic interactions between constituent particles (such as drops, rigid objects and cells) play a critical role shaping the overall rheology of an emulsion or a suspension [7-10]. Numerical investigations of concentrated suspensions of capsules have shown that interactions between capsules influence the rheology [5,8,11] giving rise to shear thinning [12,13] or a layered structure [14]. Viscosity ratio was also seen to be an important factor in dynamics—a stable aggregate is shown to form only at higher cytoplasmic viscosity and membrane rigidity [15]. Understanding pairwise interactions between capsules is the first step towards a complete theory of multi-capsule systems. Barthes-Biesel and coworkers [16,17] simulated pair-collision between homogeneous capsules in a shear, analyzing post-collision increase in cross-stream separation. The separation was found to weakly depend on the capillary number. The authors also observed that capsules placed in different shear planes can lead to a net negative deflection in the vorticity direction [18]. The magnitude of the net negative deflection in the vorticity direction is lower than the shear direction [19]. Size of the computational domain and boundary conditions were seen to critically affects capsule trajectory; smaller periodic domain in flow direction led to spiraling trajectories [20,21]. For heterogeneous collisions between a pair of capsules, simulations have noted that the stiffer capsule experiences larger cross-stream displacement [22,23]. There have been subsequent hydrodynamic Monte-Carlo simulation of a binary suspension of stiffer and floppier capsules in a confined system investigating the role of heterogeneity in the margination process [24]. However the heterogeneous collision between capsule pair has not been studied in detail, and therefore felt worthy of further investigation. We would show that how properties of one capsule affects the trajectory of the other which might have important implications in design of deformability based cell-sorting devices [25].

The effects of varying viscosity ratio on the interaction would also be investigated. For a single capsule, viscosity ratio was found to change capsule dynamics from tank-treading (TT) to trembling (TR) and eventually to tumbling (TU) motion [6,26,27]. Note that we recently investigated pair-wise collision between viscous drops in shear to find that presence of finite inertia gives rise to a reversal of trajectory [28]—an effect also seen in case of a capsule pair [20]. Increasing viscosity ratio leads to a reduced post-collision cross-stream separation for pair collision of drops in a free shear [29]. We also showed that a pair of viscous drops in a confined shear after collision comes to the center of the domain separated by a net stream-wise separation [30]. Although membrane provides very different interfacial stresses compared to those due to a drop simple drop, the similarity between drops and capsules are self-evident. Therefore, it is natural to enquire the difference in their behaviors, which has not been systematically investigated [31]. Here we offer a comparative study between pair-collisions of drops and capsules.

Here we use a front tracking finite difference method [32,33] which we have previously applied to viscous [34-38] and viscoelastic [39-45] drops as well as capsules [3,31]. The problem setup and mathematical formulation are described in section 2. In section 3, we first compare our simulation with a previous boundary element simulation for interaction between a pair of homogenous capsules. Then we study effects of viscosity ratio on homogenous capsule-interactions followed by collision between a pair of heterogeneous capsules. We analyze the effects of stiffness on relative trajectory between capsules, deformations, and lateral velocity of the capsules. In section 4, we summarize the present work.

II. Mathematical Formulation

The mathematical formulation and its front tracking implementation [32,35-37] along with constitutive equations for the membrane have been presented before [3] . Here, we provide a brief sketch of the same:

$$\nabla \cdot \mathbf{u} = 0$$
$$\frac{\partial(\rho \mathbf{u})}{\partial t} + \nabla \cdot (\rho \mathbf{u}\mathbf{u}) = -\nabla p + \nabla \cdot \left[\mu\left(\nabla \mathbf{u} + (\nabla \mathbf{u})^T\right)\right] - \int_{\partial B} \mathbf{f}^m(\mathbf{x}')\delta(\mathbf{x} - \mathbf{x}')dS(\mathbf{x}'), \quad (1)$$

where p is the pressure, ρ the density and μ the viscosity of the fluid. The density and viscosities are uniform in each phase and are allowed to have a sharp variation across the membrane ∂B separating them. In this work, the capsules are assumed to be neutrally buoyant with same density as that of the liquid outside. The superscript ^{T} represents transpose. $\mathbf{f}^m$ is the surface traction in the membrane arising as a jump in the stress condition across the membrane. The surface membrane force is written as a singular volume force using Dirac delta function $\delta(\mathbf{x} - \mathbf{x}')$; the force is present only at the boundary.

A. Membrane constitutive models

The elastic stress in the membrane is determined by the initial membrane configuration and its deformation state via two-dimensional constitutive laws. In this paper, three different laws, neo-Hookean, Skalak and Evans & Skalak are considered. The following description follows closely one of our recent publication [31]. A neo-Hookean membrane (NH) is a basic hyperelastic model that assumes the membrane to be an infinitely thin sheet of isotropic volume-incompressible elastic media. The area of the membrane is allowed to change and its change is balanced by the thinning of the membrane. Its strain-energy function is:

$$W = \frac{G_s}{2}\left(\lambda_1^2 + \lambda_2^2 + \frac{1}{\lambda_1^2 \lambda_2^2} \right), \tag{2}$$

where G_s is the shear modulus, λ_1 and λ_2 are the principal stretches on the membrane surface. The principal membrane stresses are:

$$\begin{aligned} \tau_1^m &= \frac{1}{\lambda_2}\frac{\partial W}{\partial \lambda_1} = \frac{G_s}{\lambda_1 \lambda_2}\left(\lambda_1^2 - \frac{1}{\lambda_1^2 \lambda_2^2} \right), \\ \tau_2^m &= \frac{1}{\lambda_1}\frac{\partial W}{\partial \lambda_2} = \frac{G_s}{\lambda_1 \lambda_2}\left(\lambda_2^2 - \frac{1}{\lambda_1^2 \lambda_2^2} \right). \end{aligned} \tag{3}$$

Skalak *et al* [46] proposed a constitutive model for red blood cell membrane (SK) by incorporating area-incompressibility of the membrane in the stress computations. The strain-energy function is given as:

$$W = \frac{G_s}{4}\left[\left(\lambda_1^4 + \lambda_2^4 - 2\lambda_1^2 - 2\lambda_2^2 + 2 \right) + C\left(\lambda_1^2 \lambda_2^2 - 1 \right)^2 \right]. \tag{4}$$

The first term of the energy equation is due to shear of the capsule whereas the second term involving C represents area dilation of the capsule. A large value of C (≥ 1) leads to incompressible area of membrane. The principal membrane stresses are:

$$\begin{aligned} \tau_1^m &= \frac{G_s}{\lambda_1 \lambda_2}\left[\lambda_1^2\left(\lambda_1^2 - 1 \right) + C\lambda_1^2 \lambda_2^2\left(\lambda_1^2 \lambda_2^2 - 1 \right) \right], \\ \tau_2^m &= \frac{G_s}{\lambda_1 \lambda_2}\left[\lambda_2^2\left(\lambda_2^2 - 1 \right) + C\lambda_1^2 \lambda_2^2\left(\lambda_1^2 \lambda_2^2 - 1 \right) \right]. \end{aligned} \tag{5}$$

Evans and Skalak [47] simplified the above constitutive model by adding linearly and independently contributions of the shear and dilations (denoted by ES). The principle membrane stresses are:

$$\begin{aligned} \tau_1^m &= G_S\left[\frac{1}{2\lambda_1^2 \lambda_2^2}\left(\lambda_1^2 - \lambda_2^2 \right) + A\left(\lambda_1 \lambda_2 - 1 \right) \right], \\ \tau_2^m &= G_S\left[\frac{1}{2\lambda_1^2 \lambda_2^2}\left(\lambda_2^2 - \lambda_1^2 \right) + A\left(\lambda_1 \lambda_2 - 1 \right) \right], \end{aligned} \tag{6}$$

At C =1 and A = 3, the NH, SK and ES model shows same deformation of a capsule in at small deformation regime but they show nonlinear stress-strain relation in large deformation [48].

B. Numerical implementation

Two equal sized initially spherical capsules with radius a are placed symmetrically in the computational domain with initial separations $\Delta x_0 / a$, $\Delta y_0 / a$ and $\Delta z_0 / a$ in the three directions (Figure 1). Periodic boundary conditions are imposed in the flow (x) and the vorticity (z) directions. The top and the bottom walls of the domain move in opposite directions with velocity U and $-U$ respectively, resulting in a simple shear (with rate $\dot{\gamma}$ in y-direction). We use a domain size of $30a \times 30a \times 5a$ for cases when both capsules are in the same shear plane with a discretization level of 288×288×48 and 20480 elements on the surface of each capsule. We use the radius of the capsules a as the length scale and the inverse shear rate $\dot{\gamma}^{-1}$ as the timescale to define dimensionless parameters for the problem: Reynolds number $\mathrm{Re} = \rho_m \dot{\gamma} a^2 / \mu_m$, elastic capillary number $Ca = \mu_m \dot{\gamma} a / G_s$, viscosity ratio $\lambda = \mu_c / \mu_m$. For the case of drops, we use a capillary number $Ca = \mu_m \dot{\gamma} a / \Gamma$, where Γ is the interfacial tension. Subscripts m and c stands for matrix and capsules. Note that the explicit nature of the code prevents us from simulation in the Stokes limit. We use a small Reynolds number of Re = 0.01 as an approximant for Stokes flow in this paper.

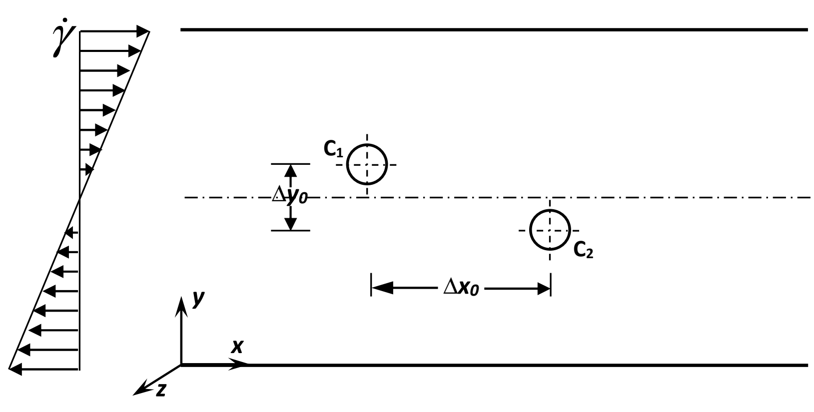

Figure 1: A Schematic of the computational domain showing the initial position of the pair of capsules.

III. Results and Discussions

In this section, we present results of our numerical simulations for hydrodynamic interactions between a pair of capsules in the free shear in a domain $30a \times 30a \times 5a$ after briefly examining the validity of the code. We analyze results for trajectory of individual capsule, relative trajectory between capsules as well as deformation and lateral velocity of the capsules. Unless otherwise specified, the capsules are enclosed with a NH membrane. We also compare with results from interactions between a pair of drops. Assuming an approximate ellipsoidal shape of the capsule/drop, we compute Taylor deformation $D = (L - B) / (L + B)$ from numerically computed capsule/drop shapes (L and B are the major and the minor axes of the ellipsoid).

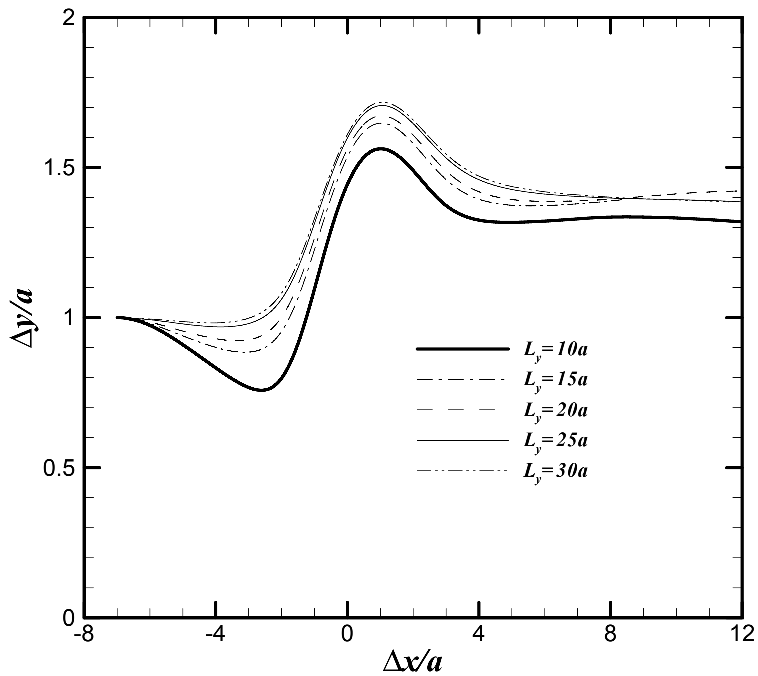

Figure 2: Relative trajectory of a pair of capsules at $Ca = 0.30$, $\Delta x_0 / a = 7$ and $\Delta y_0 / a = 1$ in different computational domains.

A. Effects of domain size and validation

Although our objective is to simulate pair collision in free shear, the computational domain is bounded. Domain size affects the simulated dynamics; small domain with periodic boundary condition in the flow direction has shown to result in spiraling trajectories [20,21] due to interactions between one capsule coming close to the periodic image of the other. They cannot be found in free shear. We have previously shown that a domain size of $L_x = 30a$ is sufficient to achieve a net cross-stream separation between a pair of drops before they reach the boundary [29]. Small domain size in the shear direction also leads to lateral migration of a drop away from the bounded wall [30]. Confinement was also shown to result in wall induced lateral motion of drops and rigid

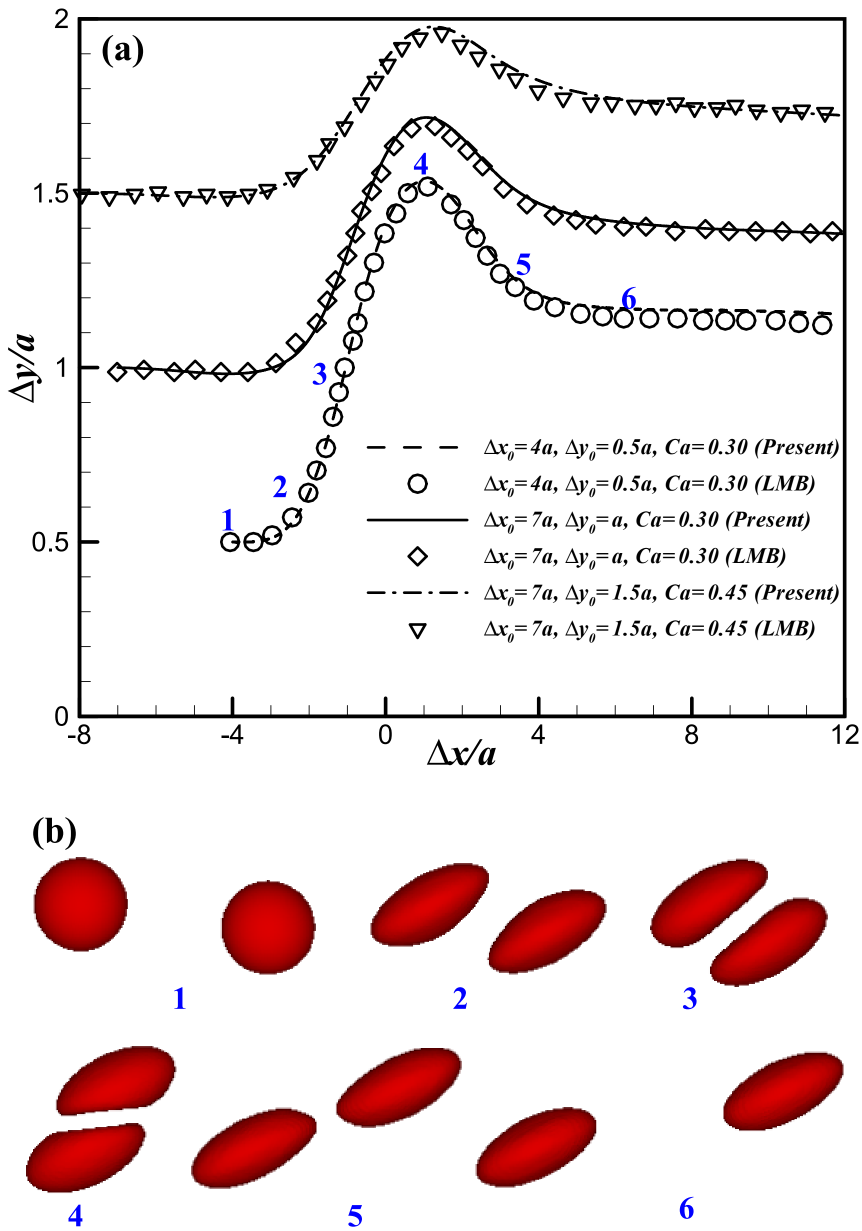

Figure 3: (Color online) (a) Comparison of the simulated relative trajectory of pair of capsules with boundary element simulation of Lac et al, 2007, (LMB in figure) at $\lambda = 1$, different initial separations and Ca values. (b) Simulated snapshots of the pair of capsules at the instants shown in (a) for $\Delta x_0/a = 4$ and $\Delta y_0/a = 0.50$.

spheres post collision giving rise to swapping [49] or reversed trajectories [28]. In Figure 2, we study the effects of domain size in the shear direction on the relative trajectory of a pair of capsules. For $L_y \geq 25a$, relative trajectory of the capsules does not vary with further increase in domain size, and after collision achieves a final value of $\Delta y/a$. However, in smaller domains, wall confinement leads to lateral motion of the capsules before and after collision. We conclude that the domain size $30a \times 25a \times 5a$ chosen here is sufficient to simulate the pair collision of capsules in free shear.

We also compare our simulations with results in the literature. In our previous study, we compared deformation, orientation angle and tank treading period of a single capsule in free shear [3] with analytical results for small deformation [4,50] and Boundary Element Method (BEM) simulations [27]. Here, in Figure 3(a), we compare relative trajectories of colliding homogeneous capsule pair in a free shear computed here with those obtained using BEM by Lac *et al* [16]. For two different initial separations and two different capillary numbers (*Ca* = 0.30, 0.45) our results match very well with those obtained using a completely different method (note that BEM does not suffer from the limitations of a bounded computational domain). Figure 3(b) shows the shapes of the capsules at six time instants during their collision.

B. Effects of viscosity ratio: different membrane laws and comparison with drops

For many cells, viscosity of the internal fluid differs from that of outside. The viscosity ratio significantly changes the deformation, orientation angle and tank trading frequency of a capsule. Higher viscosity ratio shows increased rotational flow inside the capsules, and a decreased inclination angle. Here, we study the effects of viscosity ratio (λ) variation on the collision between a pair of identical capsules for different membrane constitutive laws (neo-Hookean [51], Skalak (C=1)[46] and Evans & Skalak (A=3) [47]). Figure 4(a) plots the deformation of one of them (both behaving identically) as a function of their flow-wise separation $\Delta x / a$. We choose a moderate capillary number *Ca*=0.3. The capsules initially separated by $\Delta y_0 / a$ in the shear direction are driven towards each other (see Figure 3). During their approach, they press against each other in the compression quadrant—the imposed shear flow is a combination of planar extension and rotation with compression axis oriented at 135° from the flow direction. Due to the interaction between capsules in the compression quadrant, the deformation sharply increases. Subsequently, the capsules pass each other and in the extensional quadrant

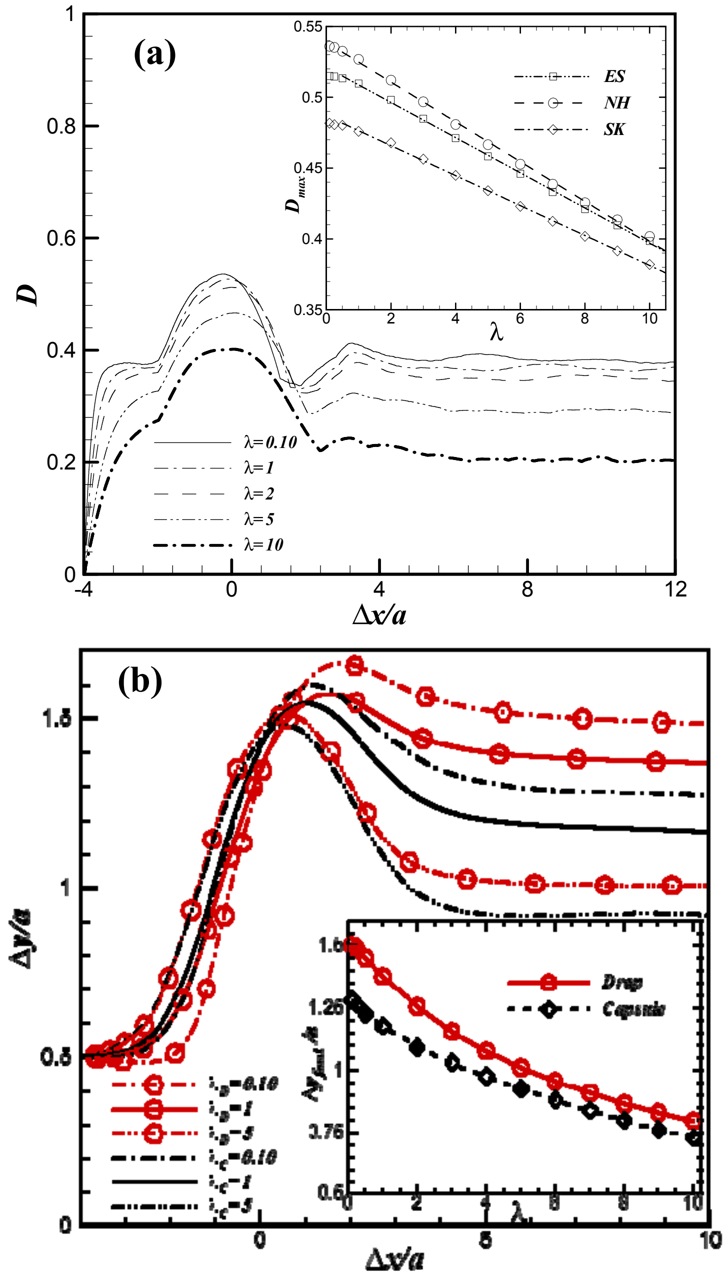

Figure 4 (Color online) (a) Deformation vs $\Delta x/a$ of a pair of NH capsules at $Ca = 0.30$, $\Delta x_0/a = 4$, $\Delta y_0/a = 0.5$ and different λ ($D_{\max}$ as a function of λ for three constitutive laws in the inset, A= 3 for ES, C=1 for SK). (b) Relative trajectories for an NH capsule pair and a drop pair for the same conditions and different λ. Inset shows the variation of $\Delta y_{final}/a$ as a function of λ for the drop and the capsule pairs.

(extensional axis is oriented at 45° to the flow direction) they separate with deformation decreasing during relaxation. At large separation, capsules achieve their equilibrium deformation. As for a single drop or capsule, the deformation is inhibited by increasing viscosity ratio. In the inset of Figure 4(a), we show that an almost linear decrease of maximum deformation with viscosity ratio is a feature common to different membrane constitutive equations. Note that Skalak model represents strain hardening and results in the smallest deformation. In contrast, NH and ES models result in very similar behaviors with values for NH slightly less than those of ES as was also seen in our earlier publication [31].

In Figure 4(b), we investigate the effects of the viscosity ratio on the relative trajectory—$\Delta y / a$ as a function of $\Delta x / a$—of a pair of Neo-Hookean capsules under same conditions. Post-collision, the pair achieves a net cross-stream separation $\Delta y_{final} / a$. $\Delta y_{final} / a$ decreases as the viscosity ratio increases as was also seen for interactions between pair of viscous drops in shear [29]. Increased viscosity ratio results in decreased deformation and quick alignment with the flow, i.e. reduced inclination angle. Note that the interactions start earlier along the approach trajectory at increasing viscosity ratio, and leads to reduced cross-stream displacement.

Figure 4(b) also plots the relative trajectories for a colliding pair of viscous drops under the same condition for comparison. Effects of viscosity ratio on the pair collision of viscous drops were studied before in a Stokes flow [52] as well as in presence of finite inertia [29]. The cross-stream separation for the capsules is smaller than that of the drops for each viscosity ratio. The inset shows that $\Delta y_{final} / a$ for capsules is smaller than that of drops (this is found for other capillary numbers, but not shown here). Note that the difference of $\Delta y_{final} / a$ between the drop and the capsule cases decreases with increasing λ. At very large viscosity ratios ($\lambda \geq 25$, not shown here), both will result in the same $\Delta y_{final} / a$, as viscous effects dominate over interfacial effects and eventually one obtains the rigid particle limit of zero $\Delta y_{final} / a$.

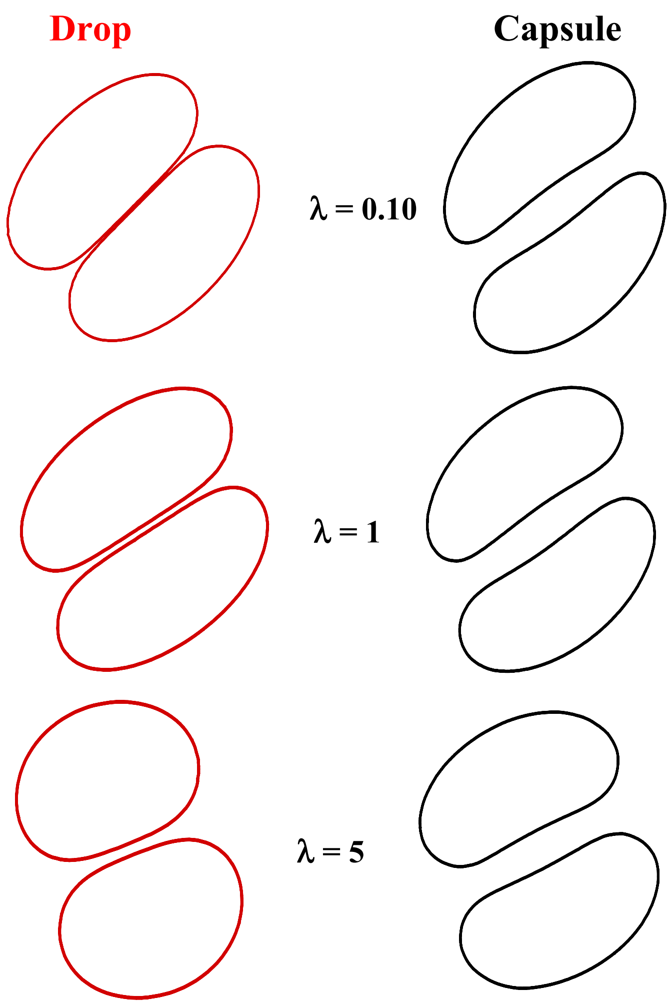

Figure 5: (Color online) Shape of capsules (NH) and drops at Ca=0.3 and different λ when they are in closest proximity in the compression quadrant.

In the compression quadrant, when a capsule- or drop-pair presses each-other, a viscous film appears in the gap between them. Figure 5 compares drop and capsule cases for different viscosity ratios at their closest encounters. Here, the capsule viscosity plays a role. Unlike in deformable drops, film thickness, in case of a pair of capsules, does not change significantly with increasing viscosity ratio. A lower value of λ results in a higher elongation of the capsule; eventually the liquid films widens. The hydrodynamic lubrication pressure eventually causes the membrane to form a dimple. Higher viscosity of the internal fluid resists the deformation and eventually the dimple reduces with increasing viscosity ratios. Interaction effects on drop trajectory are lesser than those for

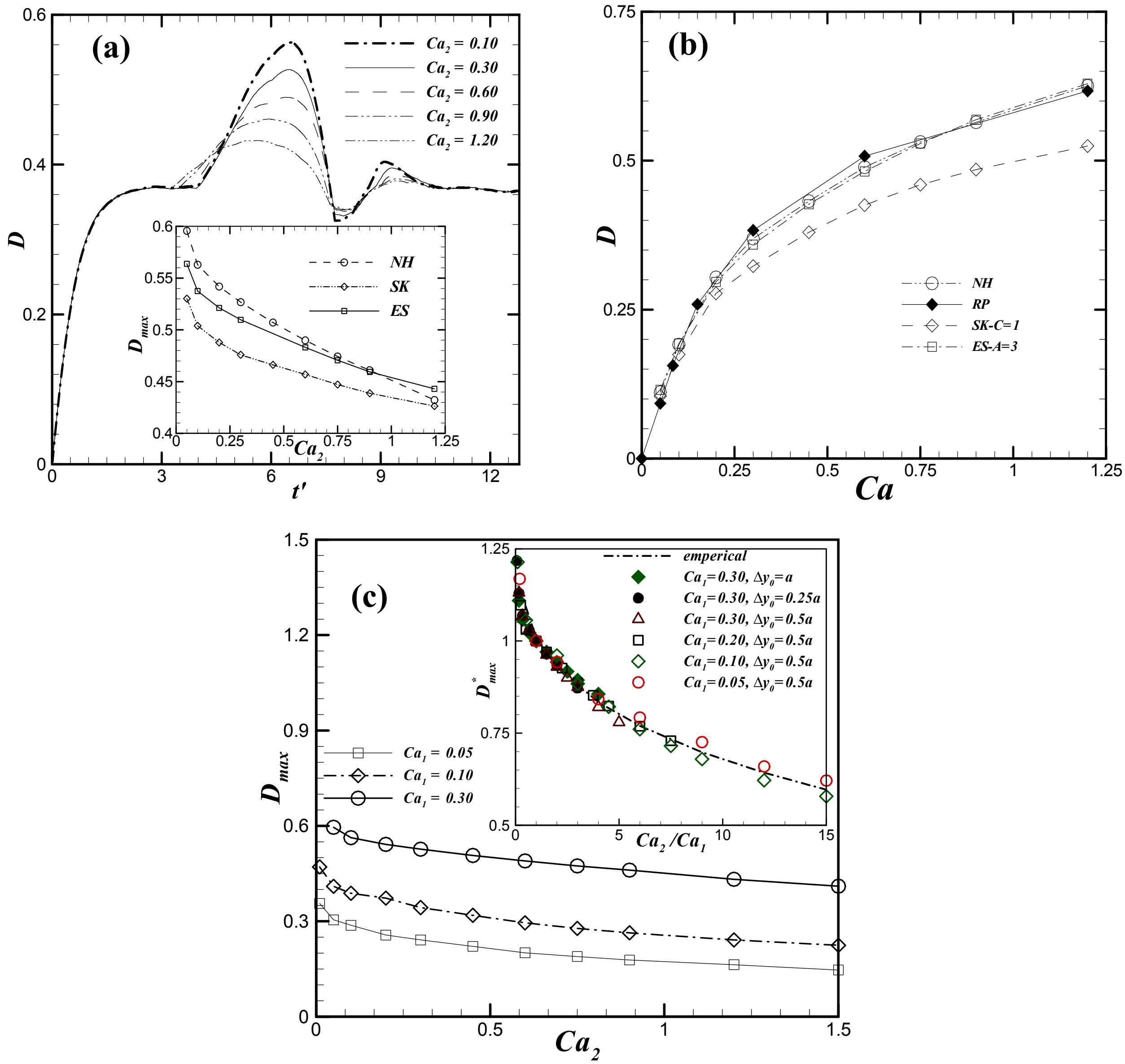

Figure 6: (a) Effect of the stiffness of C_2 on the deformation of C_1 ($Ca_1 = 0.3$). both NH capsules. Inset shows the variation of the $D_{\max}$ with Ca_2 for different models (A=3 for ES, C=1 for SK). (b) Comparison of deformation of a single NH capsule for different constitutive laws with BEM simulation of Ramanujan & Pozrikidis (1998). (c) Variation of $D_{\max}$ with Ca_2 for different Ca_1 for NH capsule pairs. Inset shows the scaling for $D^*_{\max}$ with Ca_2/Ca_1 along with the empirical fit equation (8).

capsules (Figure 5). Note that previous BEM simulation has demonstrated that the film thickness widens with increasing capillary number[16].

Different membrane constitutive laws do not affect the capsule dynamics drastically as was also noted before in BEM simulation [17]. Note that NH is a strain softening model under large deformation. On the other hand, SK is a strain hardening model that produces large stresses in same deformation [51]. Later, we will explain the effects of area-dilation modulus in the Skalak models on pair interactions.

C. Heterogeneous collisions: effects of membrane stiffness and comparison with drops

As mentioned before, many diseases results from change in cell membrane stiffness. In this subsection, we investigate collisions between capsules with different membrane stiffness, or in non-dimensional terms, with two different capillary numbers $Ca_1 = \mu\dot{\gamma}a/G_{S1}$ for capsule C_1 and $Ca_2 = \mu\dot{\gamma}a/G_{S2}$ for capsule C_2. We fix the stiffness of C_1 ($Ca_1 = 0.3$) and vary the stiffness of C_2 (i.e. Ca_2) to see its effects on the dynamics of C_1, and repeat the study for different Ca_1. Henceforth, the results such as deformation D or drift $\delta \mathrm{y} = (y - y_0)$ will always correspond to those of C_1. The hydrodynamic interactions between a pair of capsules are dictated by the flow-field. When stokes number ($\rho_c\dot{\gamma}a^2/\mu_m$) of the capsule is very small (= 0.01 in the present study), capsule tends to follow the streamlines in the flow field.

In Figure 6(a), we plot the temporal evolution of the deformation of C_1 for different Ca_2. As expected, long time after collision $\Delta x/a \geq 5$, hydrodynamic interactions between the capsules become negligible, and deformation of C_1 does not change with further increase of Ca_2. However, the peak deformation $(D_{\max})$ of C_1, when both capsules press each other in the compression quadrant, decreases with increasing Ca_2, which at first seems surprising. One can understand this by noting that the excess deformation of C_1 arises due to interactions with C_2; the presence of C_2 is felt by the viscosity mismatch inside C_2 and the interfacial elastic force at its surface. In the present viscosity matched case, the elastic membrane force represented by Ca_2 is the only effect. Decreasing it, i.e. increasing the C_2 membrane stiffness, increases its effects on the flow that deforms C_1. However, also note that decreasing Ca_2 also decreases the deformation of C_2, and thereby decreases its effects on the flow field. Competition between the two effects would determine the dynamics. Here we find that the first effect outweighs the second giving rise to increasing D with decreasing Ca_2. In the Appendix, we offer an analytical argument for the deformation of C1 $D_{\max} \sim 1/Ca_2$.

We compare peak deformation of the capsule for different constitutive models—NH, ES (A=3) and SK (C=1)—in the inset of Figure 6(a). At low Ca_2, and correspondingly higher D, we notice higher difference in $D_{\max}$ from one membrane model to the next, but it shows nearly the same value for NH and ES membrane at higher deformation. The Skalak model [46] shows the lowest deformation. To understand this, we plot the deformation of a single capsule in free shear for these models for different Ca values in Figure 6(b). Deformation of NH and ES capsules matches well with BEM simulations of Ramanujan & Pozrikidis (RP) [27]. In contrast, despite the same value of G_S (C=1), Skalak model results in a smaller deformation. Note that computation of membrane force is based on the modulus of rigidity of membrane while RP computed this by Young's modulus. For NH membrane $\nu = 0.5$ leads to $E_h = 2(1+\nu)G_s = 3G_s$ and therefore our computed $Ca_{NH} = 3Ca_{RP}$. Similarly, for SK model, $\nu = C/(1+C)$ and $C = 1$, $G_{SK} = G_{NH} = E_h/3$.

We also compare the variation of $D_{\max}$ with Ca_2 for different Ca_1 in Figure 6(c). $D_{\max}$, as expected, increases with increasing Ca_1. One could also on dimensional ground argue that $D_{\max}$ depends on both Ca_1 and Ca_2. We further normalize $D_{\max}$ by its value for a homogeneous collision, $D_{\max}^{\text{homo}}$ corresponding to $Ca_2 = Ca_1$ (and therefore the same value for both capsules). Empirically we find the following relation from our simulations

$$D_{\max}^{*} = D_{\max} / D_{\max}^{\text{homo}} = 1.40\left\{1 - 0.28\left(Ca_2/Ca_1\right)^{0.275}\right\}. \qquad (7)$$

The relation is shown in the inset of Figure 6(c) to collapse simulations from many different Ca_1 and Ca_2 to a single curve. Even different initial vertical separations Δy_0 collapse on the same curve indicating the robustness of the relation. Note that the relation recovers the value of maximum homogeneous deformation for $Ca_2 = Ca_1$. In the

Appendix, we explore possible reasoning behind the Ca_1 / Ca_2 scaling. Please note that the relation (7) is restricted to viscosity matched system.

In Figure 7(a), we plot the trajectory of the center of capsule C_1 for different Ca_2 to see that the deformability of C_2 also affects the trajectory of the capsule C_1. However, we note that the cross-streamline excursion $\delta y = (y - y_0)/a$ of C_1 increases with increasing Ca_2. Note that δy represents excursion of one capsule C_1 from its original location while Δy represents relative separation between C_1 and C_2. Above, we recognized two competing ways C_2 can affect C_1. Here the second effect dominates, viz., increasing Ca_2 increases deformation of C_2, which in turn changes the flow around C_1 increasing its lateral drift. One can see that the maximum lateral drift $\delta y_{\max}$ of C_1 increases with increasing Ca_2. An alternative explanation for the same observation was offered in [53] in view of the dominating effects of the lubrication pressure in the contact dynamics—the floppy particle deforms in response to the lubrication pressure whereas the stiffer particle must displace. In Figure 7(b), we notice that the net drift (δy_{final}) increases with Ca_2, but decreases with increasing Ca_1. However, the variation with Ca_2 has different scalings for low and high Ca_1. At low Ca_1 (Ca_1<0.1) $\delta y_{final}/a \sim Ca_2$ (inset of Figure 7b), but for Ca_1 ≥ 0.1, $\delta y_{final}/a \sim Ca_2^{0.6}$. Although completely different phenomenon, we parenthetically note that 0.6 power scaling of Ca was also found previously for lateral migration of capsules in free shear [54,55]. Similar to the deformation, we could obtain an empirical relation by normalizing it with the value for homogeneous collision

$$\begin{aligned} \delta y^*_{final} &= \frac{\delta y_{final}}{\delta y^{\text{homo}}_{final}} = \left\{0.97 + 0.028\left(Ca_2 / Ca_1\right)\right\} \qquad Ca_1 < 0.1 \\ \delta y^*_{final} &= \frac{\delta y_{final}}{\delta y^{\text{homo}}_{final}} = \left\{0.65 + 0.33\left(Ca_2 / Ca_1\right)^{0.6}\right\} \qquad Ca_1 \geq 0.1 \end{aligned} \tag{8}$$

Results are shown in Figure 7(c) with different Ca_1 and Ca_2 collapse on to a single curve for both regimes (see also the inset of Figure 7c). Again as in deformation, different initial separations fall on the same curve making the relation independent of initial configuration.

Although, stiffness of the second particle is shown to have significant effects on

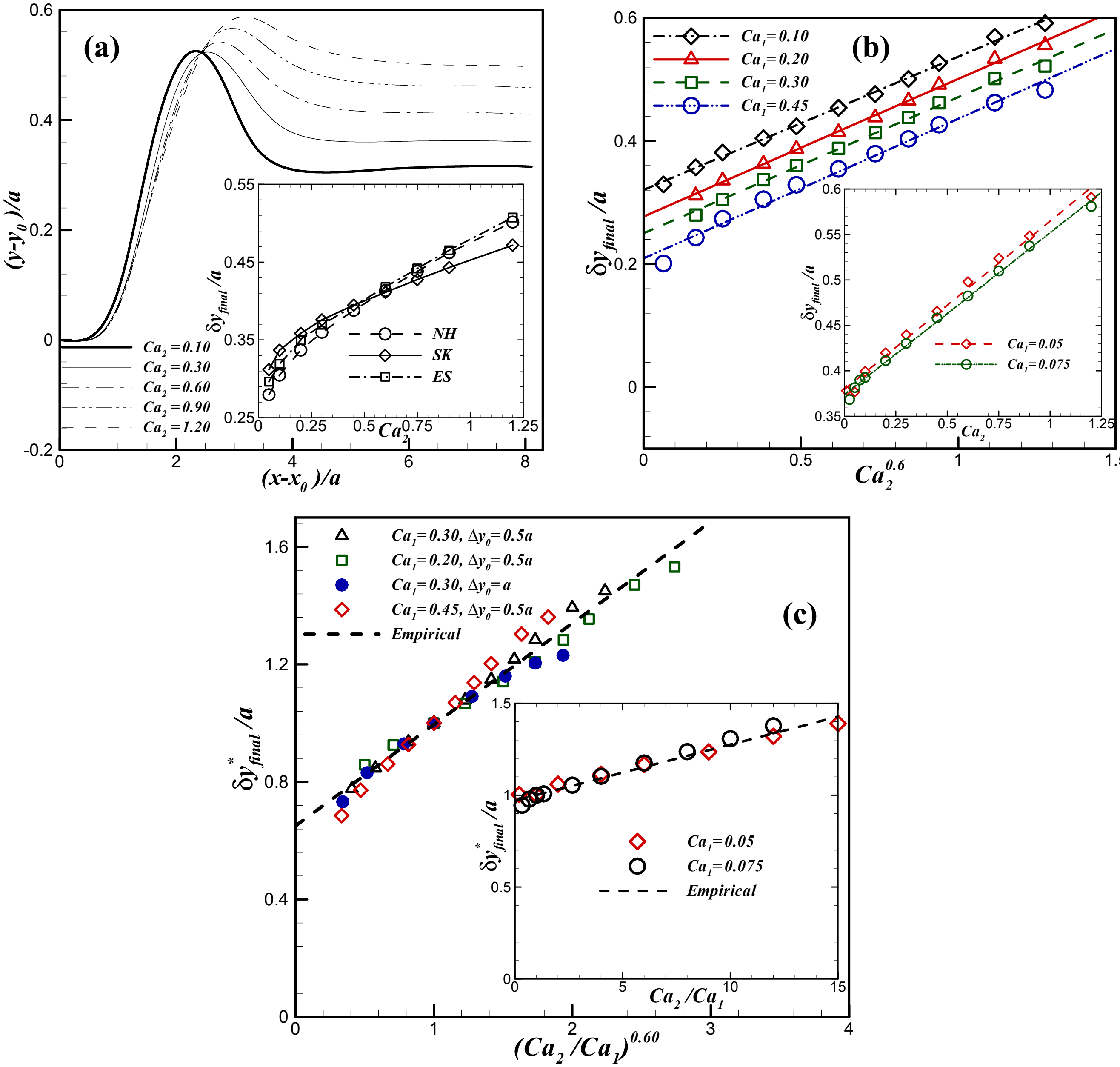

Figure 7: (Color online) (a) Effect of Ca_2 on the trajectory of C_1 for an NH capsule pair. Inset shows $\delta y_{final}/a$ of C_1 for different constitutive laws (ES *A*=3, SK *C*=1). (b) $\delta y_{final}/a$ versus $Ca_2^{0.60}$ for $Ca_1 \geq 0.10$. The Inset shows variation of $\delta y_{final}/a$ with Ca_2 for $Ca_1 < 0.10$. (c) Empirical expression (9) plotted along with simulated results for $Ca_1 > 0.10$. The inset shows same plot for $Ca_1 < 0.10$.

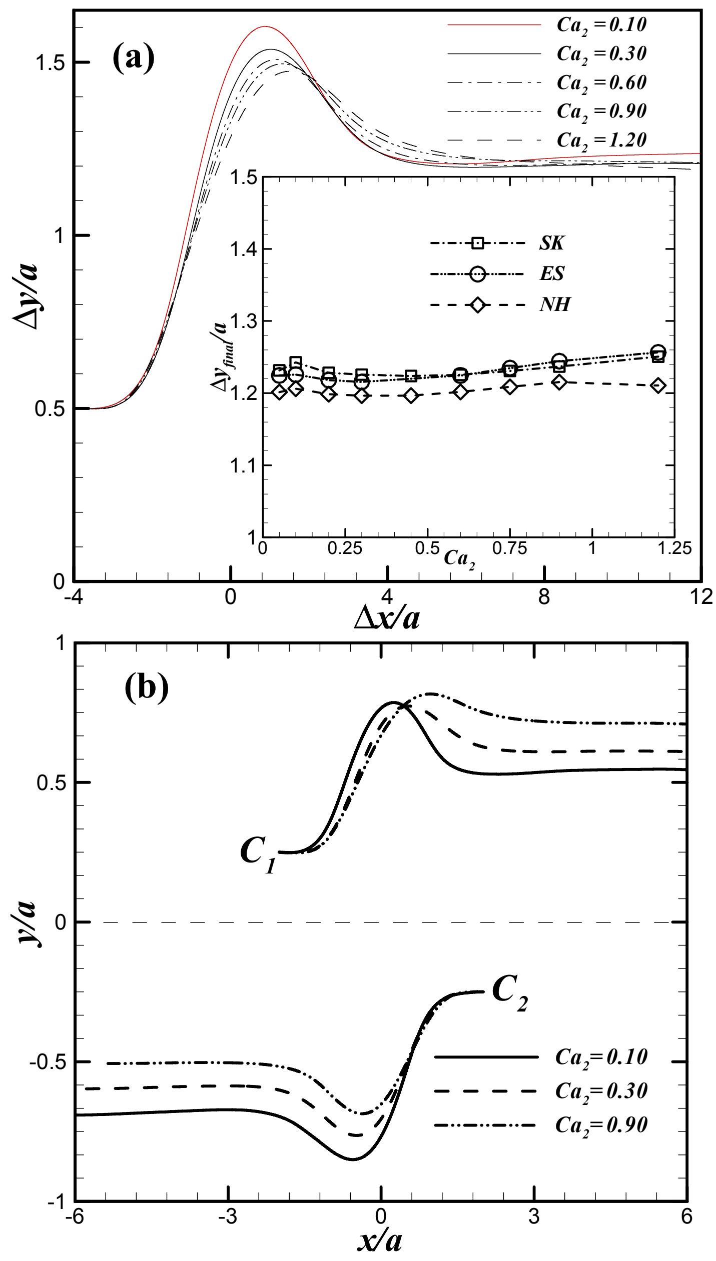

Figure 8: (Color online) (a) Relative trajectory of a pair of heterogeneous NH capsules at $Ca_1 = 0.3$ and different Ca_2. Inset shows the variation of $\Delta y_{final}/a$ with Ca_2 for different constitutive laws (ES A=3, SK C=1) at $Ca_1 = 0.3$. (b) Trajectories of the centers of capsules for three Ca_2 at $Ca_1 = 0.3$.

particle trajectory (Figures 7), the relative trajectory $\Delta y/a$ as a function of $\Delta x/a$ shown in Figure 8(a), especially its final value, remains insensitive (see Figure 8a inset). It can be understood from Figure 8(b), where we see that although the lateral drift of C_1 increases with Ca_2, that of C_2 concurrently decreases leaving the relative displacement unchanged. Note that in a heterogeneous collision, the stiffer particle experiences larger drift velocity [20]. Figure 8(b) accordingly shows that for $Ca_2 = 0.1$, C_2 moves faster than C_1, whereas for $Ca_2 = 0.9$, C_1 moves faster. The inset of Figure 8(a) plots $\Delta y_{final}/a$

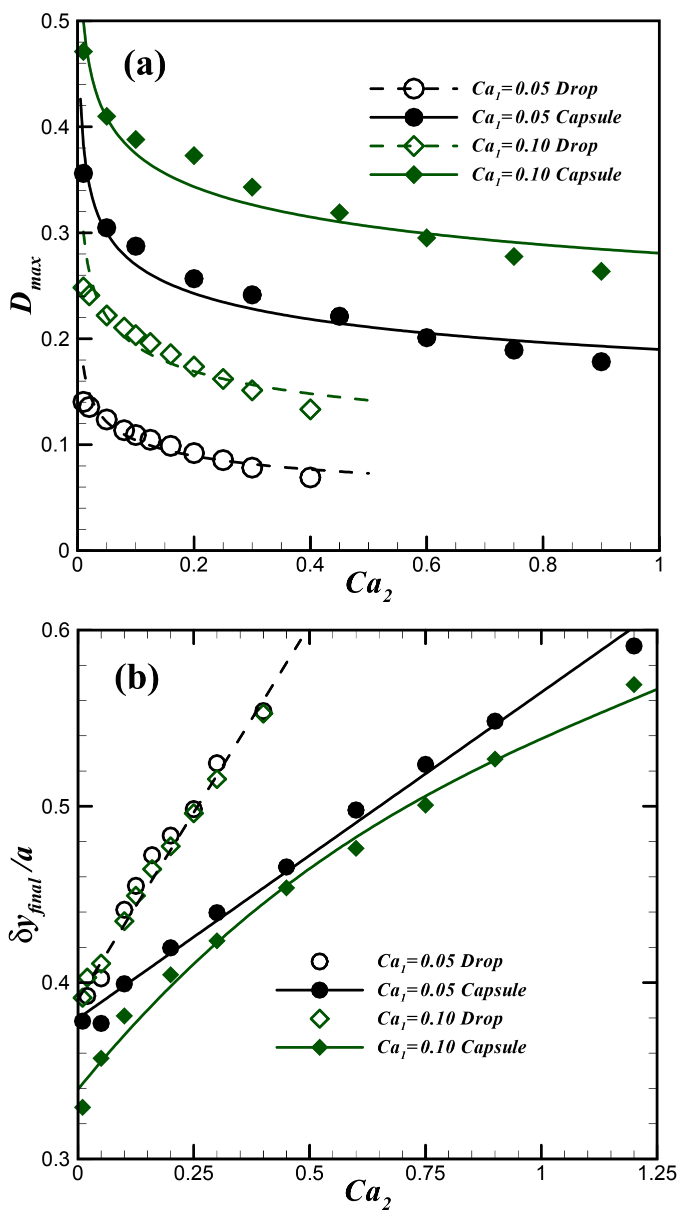

Figure 9: (Color online) (a) Comparison of the variation of $D_{\max}$ with Ca_2 for pair collision of drops and capsules. Comparison of $\delta y_{final}/a$ between Drop and Capsule at two Ca_1 values.

vs. Ca_2 for different constitutive laws showing nearly identical results for the NH and ES models, whereas the SK model shows slightly smaller drift. The difference in behaviors for the strain hardening SK (Skalak) model from NH model even for the same value of G_s has been previously observed [51]. The area dilation modulus C affects the deformation and thereby the overall dynamics, which we investigate below.

We also simulate heterogeneous collision between a pair of drops to compare the capsule and drop dynamics under collision. In Figure 9(a), $D_{\max}$ for C_1 as a function of Ca_2 shows similar dynamics for different values of Ca_1 for both drops and capsules. However, the drop deformation is smaller than that of the capsule for the same values of Ca_1 and Ca_2. Previously, we found that a single capsule in deforms more than a drop in simple shear [31]. Note that the capillary number used here is a ratio of approximate measures of viscous to capillary forces for a drop and viscous to elastic membrane forces for a capsule. The actual forms of capillary and membrane stresses are different. At zero deformation, the drop experiences surface tension in contrast to a capsule, which experiences no stress. Therefore, the restoring force is stronger in case of a drop than in the capsule. In Figure 9(b) $\delta y_{final}/a$ for drop and capsule cases are plotted for two different Ca_1 values. $\delta y_{final}/a$ shows linear variation with Ca_2 for Ca_1=0.05. For a larger value Ca_1=0.1, although the drop case still shows linear variation, the capsule case displays nonlinear variation as also seen above $\left(\sim Ca_2^{0.6}\right)$ for $Ca_1 \geq 0.1$ (Figures 7b and 7c).

D. Effects of area dilatational modulus in Skalak model

The Skalak model is characterized by the area dilation coefficient C apart from G_s. In Figure 10(a), we investigate its effects on the homogenous pair interaction for Ca =0.3. $\Delta y/a$ increases with increasing value of C. It grows quicker at lower values of $C(\leq 1)$, and then seems to achieve an asymptotic value independent of C for larger C (inset of Figure 10a). Larger values of C leads to a nearly incompressible membrane with area dilation modulus $K_S = G_S\left(1+2C\right)$ dominating over the shear modulus [51]. Indeed deformation was shown in that article to reach an asymptotic value at large C. Deformability affects trajectory explaining the C independent results here. A related effect of the strain hardening behavior of the Skalak model is that it prevents capsule from bursting even at large Ca values.

We investigate heterogeneous collisions between capsules C_1 and C_2 of two different capillary numbers $Ca_1 = 0.3$ and Ca_2 but same C in Figure 10(b). It plots net lateral drift $\delta y_{final}/a$ of C_1 for different C as a function of Ca_2 for Ca_1=0.3. At low Ca_2, C affects the drift more—it increases with increasing C, but at high Ca_2,

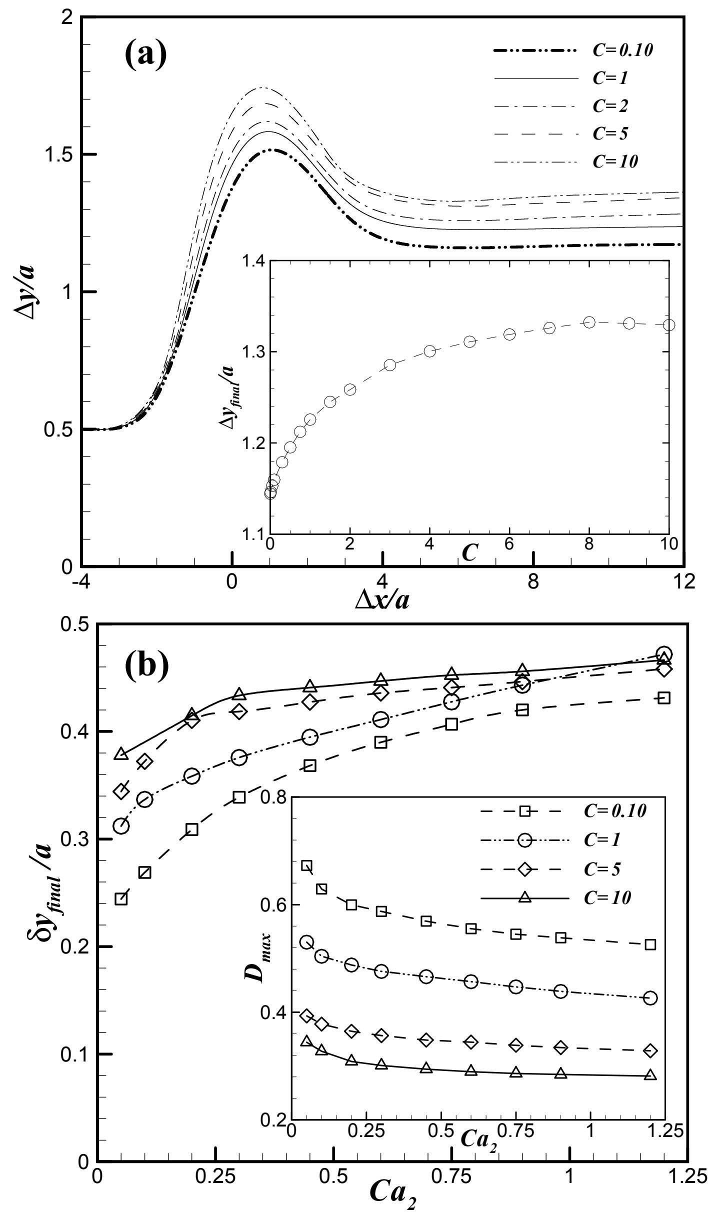

Figure 10: Relative trajectory of a pair of capsules in homogenous collision at different C for Skalak model at $Ca = 0.3$, x_0/a=4 and $y_0/a = 0.5$. Inset shows the variation of $\Delta y_{final}/a$ with *C*. (b) Effect of C on the variation of $\delta y_{final}/a$ of the C_1 with Ca_2. Inset shows the plot for $D_{\max}$ of C_1 with Ca_2 at different *C*.

difference between different C is negligible. The inset shows $D_{\max}$ of C_1 with Ca_2 for different C ; it decreases with increasing C as expected.

IV. Summary

We have investigated pair interactions between capsules encapsulated by an elastic membrane described by three different hyperelastic constitutive models—neo-Hookean, Skalak and Evans and Skalak. We show excellent match of our simulated results with prior boundary element simulations of homogeneous capsule interactions. For homogeneous interactions, the maximum deformation of capsules and the net cross-stream separation $\Delta y_{final}/a$ expectedly decrease with increasing viscosity ratio λ , as $\lambda \to \infty$ one recovers reversible Stokes flow dynamics of interacting sphere-pairs. A pair of drops shows higher values of $\Delta y_{final}/a$ than those of a pair of capsules, although the difference between the drop and capsule cases disappears for very large λ. For heterogeneous collisions between two capsules C_1 and C_2, the peak deformation $D_{\max}$ of capsule C_1 decreases with increased capillary number Ca_2 of C_2, while the cross-stream drift $\delta y_{final}/a$ of capsule C_1 increases. They scale with Ca_1/Ca_2 both for capsule and drop pairs. We provide an approximate analytical argument for the observed scaling in the Appendix. While for the same conditions $D_{\max}$ is larger for capsule, $\delta y_{final}/a$ is larger for drops. Even though $\delta y_{final}/a$ of one capsule (C_1) varies with the variation of the capillary number of the other capsule (C_2), the relative shift $\Delta y_{final}/a$ does not change. Different membrane constitutive laws result in very similar behavior. The area-dilatation coefficient C in Skalak model, when increased, gives rise to reduced $D_{\max}$ and enhanced $\Delta y_{final}/a$ for the other capsule.

Acknowledgement

This work is partially supported by NSF Grants No. CBET-1205322, DMR-1239105 and George Washington University.

Appendix: Ca_1 / Ca_2 scaling for heterogeneous scaling

For heterogeneous collision between two capsules C_1 and C_2 of different capillary numbers Ca_1 and Ca_2, we find that the maximum deformation [Eq. (7)] and the final lateral shift [Eq. (8)] both experience a scaling $\sim Ca_1 / Ca_2$. Here, we explain the underlying physics and provide an approximate reasoning for the capillary dependence by investigating effects of the velocity field of one drop on the other. We express the flow field outside the capsule C_2 due to the free shear in absence of C_1 using the Stokes Green's function $G_{ij}(\mathbf{x},\mathbf{y})$ and the corresponding stress $T_{ijk}(\mathbf{x},\mathbf{y})$ as [31,56-58]

$$u_j(\mathbf{x}) = u_j^\infty(\mathbf{x}) - \frac{1}{8\pi\mu_m}\int_{A_d} f_i^m(\mathbf{y})G_{ij}(\mathbf{x},\mathbf{y})dA(\mathbf{y}) + \frac{(1-\lambda)}{8\pi}\int_{A_d} u_i(\mathbf{y})T_{ijk}(\mathbf{x},\mathbf{y})n_k(\mathbf{y})dA(\mathbf{y}),$$
$$G_{ij}(\mathbf{x},\mathbf{y}) = \frac{\delta_{ij}}{|\mathbf{x}-\mathbf{y}|} + \frac{(x_i-y_i)(x_j-y_j)}{|\mathbf{x}-\mathbf{y}|^3}, \qquad T_{ijk}(\mathbf{x},\mathbf{y}) = -6\frac{(x_i-y_i)(x_j-y_j)(x_k-y_k)}{|\mathbf{x}-\mathbf{y}|^5}. \tag{9}$$

For the case of viscosity matched system ($\lambda = 1$) the second term drops out. u_i^∞ is the imposed shear. A_d is the surface of the capsule C_2 with outward normal $n_i(\mathbf{x})$. $f_i^m(\mathbf{x})$ is the membrane force appearing in (1) that also is equal to the jump in fluid traction across the membrane. Note that for the case of a drop pair this membrane force $\mathbf{f}^m$ will be replaced by the appropriate jump in the traction, namely the surface tension $\mathbf{f} = \Gamma(\nabla \cdot \mathbf{n})\mathbf{n}$. After nondimensionalizing the velocity by $\dot{\gamma}a$, and the membrane traction by $G_{s,2}/a$ ($G_{s,2}$ is the membrane shear modulus of capsule C_2) the equation (9) for the velocity outside C_2 to be

$$\frac{u_j}{\dot{\gamma}a}(\mathbf{x}) = \frac{u_j^\infty}{\dot{\gamma}a}(\mathbf{x}) + \frac{u_j^{C_2}}{\dot{\gamma}a}(\mathbf{x}),$$
$$\frac{u_j^{C_2}}{\dot{\gamma}a}(\mathbf{x}) = -\frac{1}{8\pi Ca_2}\int_{A_d} \frac{f_i^m}{G_s/a}(\mathbf{y})\frac{G_{ij}}{1/a}(\mathbf{x},\mathbf{y})\frac{dA}{a^2}(\mathbf{y}). \tag{10}$$

Therefore the velocity due to C_2 shows to be scaling as $\propto 1/Ca_2$. The deformation and lateral motion of Capsule C_1 is effectively controlled by the imposed shear and this velocity due to their mutual interactions. In principle, one can compute now the velocity and deformation of C_1 and then develop a method of reflection to correct the velocity field and deformation of C_2 and so on. For our purpose just the zeroth order result is sufficient. In that order the extensional part of the velocity (10) would govern the deformation of C_1. Based on Taylor's theory of small deformation in the low Ca_1 limit one obtains deformation of C_1,

$$D \sim Ca_1 \times (\text{velocity due to } C_2) \sim Ca_1 / Ca_2 \,, \qquad (11)$$

especially when it is scaled by its reference value for homogeneous collision. One can argue that the lateral drift follows deformation and shows similar scaling.

References

[1] C. D. Eggleton and A. S. Popel, Physics of Fluids **10**, 1834 (1998).

[2] B. M. Cooke, N. Mohandas, and R. L. Coppel, in *Advances in Parasitology* (Academic Press, 2001), pp. 1.

[3] X. Y. Li and K. Sarkar, Journal of Computational Physics **227**, 4998 (2008).

[4] D. Barthesbiesel, J Fluid Mech **100**, 831 (1980).

[5] J. R. Clausen and C. K. Aidun, Physics of Fluids **22** (2010).

[6] H. Zhao and E. S. G. Shaqfeh, J Fluid Mech **674**, 578 (2011).

[7] G. K. Batchelor, J Fluid Mech **41**, 545 (1970).

[8] G. Breyiannis and C. Pozrikidis, Theor Comp Fluid Dyn **13**, 327 (2000).

[9] M. Loewenberg and E. J. Hinch, J Fluid Mech **321**, 395 (1996).

[10] T. Omori, T. Ishikawa, Y. Imai, and T. Yamaguchi, Comput Mech **54**, 933 (2014).

[11] P. Bagchi and R. M. Kalluri, J Fluid Mech **669**, 498 (2011).

[12] J. R. Clausen, D. A. Reasor, and C. K. Aidun, J Fluid Mech **685**, 202 (2011).

[13] R. Pal, Journal of Biomechanics **36**, 981 (2003).

[14] M. H.-Y. Tan, D.-V. Le, and K. H. Chiam, Soft Matter **8**, 2243 (2012).

[15] P. Bagchi, P. C. Johnson, and A. S. Popel, J Biomech Eng-T Asme **127**, 1070 (2005).

[16] E. Lac, A. Morel, and D. Barthes-Biesel, J Fluid Mech **573**, 149 (2007).

[17] P. Pranay, S. G. Anekal, J. P. Hernandez-Ortiz, and M. D. Graham, Physics of Fluids **22**, 123103 (2010).

[18] E. Lac and D. Barthes-Biesel, Physics of Fluids **20** (2008).

[19] P.-Y. Gires, A. Srivastav, C. Misbah, T. Podgorski, and G. Coupier, Physics of Fluids (1994-present) **26**, 013304 (2014).

[20] S. K. Doddi and P. Bagchi, International Journal of Multiphase Flow **34**, 375 (2008).

[21] D. V. Le and K. H. Chiam, Phys Rev E **84** (2011).

[22] A. Kumar and M. D. Graham, Phys Rev E **84**, 066316 (2011).

[23] P. Bagchi, *Computational hydrodynamics of capsules and biological cells* (CRC Press, Boca Raton, 2010), Chapman and Hall/CRC mathematical and computational biology series, p.^pp. 149-173.

[24] A. Kumar and M. D. Graham, Physical Review Letters **109**, 5, 108102 (2012).

[25] R. Quek, D. V. Le, and K. H. Chiam, Phys Rev E **83** (2011).

[26] A. Z. K. Yazdani, R. M. Kalluri, and P. Bagchi, Phys Rev E **83** (2011).

[27] S. Ramanujan and C. Pozrikidis, J Fluid Mech **361**, 117 (1998).

[28] P. O. Olapade, R. K. Singh, and K. Sarkar, Physics of Fluids **21**, 063302 (2009).

[29] R. K. Singh and K. Sarkar, Physics of Fluids **21**, 103303 (2009).

[30] K. Sarkar and R. K. Singh, Physics of Fluids (1994-present) **25**, 051702 (2013).

[31] R. K. Singh, X. Y. Li, and K. Sarkar, J Fluid Mech **739**, 421 (2014).

[32] G. Tryggvason, B. Bunner, A. Esmaeeli, D. Juric, N. Al-Rawahi, W. Tauber, J. Han, S. Nas, and Y. J. Jan, Journal of Computational Physics **169**, 708 (2001).

[33] S. O. Unverdi and G. Tryggvason, Journal of Computational Physics **100**, 25 (1992).

[34] R. K. Singh and K. Sarkar, J Fluid Mech **683**, 149 (2011).

[35] X. Y. Li and K. Sarkar, Journal of Non-Newtonian Fluid Mechanics **128**, 71 (2005).

[36] K. Sarkar and W. R. Schowalter, J Fluid Mech **436**, 177 (2001).

[37] X. Y. Li and K. Sarkar, Physics of Fluids **17** (2005).

[38] K. Sarkar and W. R. Schowalter, Journal of Fluid Mechanics **436**, 207 (2001).

[39] K. Sarkar and W. R. Schowalter, Journal of Non-Newtonian Fluid Mechanics **95**, 315 (2000).

[40] N. Aggarwal and K. Sarkar, J Fluid Mech **584**, 1 (2007).
[41] N. Aggarwal and K. Sarkar, Journal of Non-Newtonian Fluid Mechanics **150**, 19 (2008).
[42] N. Aggarwal and K. Sarkar, J Fluid Mech **601**, 63 (2008).
[43] S. Mukherjee and K. Sarkar, Journal of Non-Newtonian Fluid Mechanics **160**, 104 (2009).
[44] S. Mukherjee and K. Sarkar, Journal of Non-Newtonian Fluid Mechanics **165**, 340 (2010).
[45] S. Mukherjee and K. Sarkar, Physics of Fluids **23**, 013101 (2011).
[46] R. Skalak, A. Tozeren, R. P. Zarda, and S. Chien, Biophys J **13**, 245 (1973).
[47] E. A. Evans and R. Skalak, *Mechanics and thermodynamics of biomembranes* (CRC Press, Boca Raton, Fla., 1980).
[48] Y. Lefebvre and D. Barthes-Biesel, J Fluid Mech **589**, 157 (2007).
[49] M. Zurita-Gotor, J. Blawzdziewicz, and E. Wajnryb, J Fluid Mech **592**, 447 (2007).
[50] D. Barthesbiesel and J. M. Rallison, J Fluid Mech **113**, 251 (1981).
[51] D. Barthes-Biesel, A. Diaz, and E. Dhenin, J Fluid Mech **460**, 211 (2002).
[52] M. Loewenberg and E. J. Hinch, J Fluid Mech **338**, 299 (1997).
[53] A. Kumar and M. D. Graham, Soft Matter **8**, 10536 (2012).
[54] R. K. Singh, X. Li, and K. Sarkar, J Fluid Mech **739**, 421 (2014).
[55] P. Pranay, R. G. Henríquez-Rivera, and M. D. Graham, Physics of Fluids (1994-present) **24**, 061902 (2012).
[56] C. Pozrikidis, *Boundary integral and singularity methods for linearized viscous flow* (Cambridge University Press, Cambridge [England] ; New York, 1992).
[57] S. Mukherjee and K. Sarkar, Journal of Fluid Mechanics **727**, 318 (2013).
[58] S. Mukherjee and K. Sarkar, Physics of Fluids **26**, 103102 (2014).

Figure Captions

Figure 1: A Schematic of the computational domain showing the initial position of the pair of capsules.

Figure 2: Relative trajectory of a pair of capsules at $Ca = 0.3$, $\Delta x_0/a = 7$ and $\Delta y_0/a = 1$ in different computational domains.

Figure 3: (Color online) (a) Comparison of the simulated relative trajectory of pair of capsules with boundary element simulation of Lac et al, 2007, (LMB in figure) at $\lambda = 1$, different initial separations and *Ca* values. (b) Simulated snapshots of the pair of capsules at the instants shown in (a) for $\Delta x_0/a = 4$ and $\Delta y_0/a = 0.50$.

Figure 4 (Color online) (a) Deformation vs $\Delta x/a$ of a pair of NH capsules at $Ca = 0.30$, $\Delta x_0/a = 4$, $\Delta y_0/a = 0.5$ and different λ ($D_{\max}$ as a function of λ for three constitutive laws in the inset, *A*= 3 for ES, *C*=1 for SK). (b) Relative trajectories for an NH capsule pair and a drop pair for the same conditions and different λ. Inset shows the variation of $\Delta y_{final}/a$ as a function of λ for the drop and the capsule pairs.

Figure 5: (Color online) Shape of capsules (NH) and drops at Ca=0.3 and different λ when they are in closest proximity in the compression quadrant.

Figure 6: (a) Effect of the stiffness of C_2 on the deformation of C_1 (Ca_1 = 0.3). both NH capsules. Inset shows the variation of the $D_{\max}$ with Ca_2 for different models (*A*=3 for ES, *C*=1 for SK). (b) Comparison of deformation of a single NH capsule for different constitutive laws with BEM simulation of Ramanujan & Pozrikidis (1998). (c) Variation of $D_{\max}$ with Ca_2 for different Ca_1 for NH capsule pairs. Inset shows the scaling for $D^*_{\max}$ with Ca_2/Ca_1 along with the empirical fit equation (8).

Figure 7: (Color online) (a) Effect of Ca_2 on the trajectory of C_1 for an NH capsule pair. Inset shows $\delta y_{final}/a$ of C_1 for different constitutive laws (ES *A*=3, SK *C*=1). (b) $\delta y_{final}/a$ versus $Ca_2^{0.60}$ for $Ca_1 \geq 0.10$. The Inset shows variation of $\delta y_{final}/a$ with Ca_2

for $Ca_1 < 0.10$. (c) Empirical expression (9) plotted along with simulated results for $Ca_1 > 0.10$. The inset shows same plot for $Ca_1 < 0.10$.

Figure 8: (Color online) (a) Relative trajectory of a pair of heterogeneous NH capsules at $Ca_1 = 0.3$ and different Ca_2. Inset shows the variation of $\Delta y_{final}/a$ with Ca_2 for different constitutive laws (ES *A*=3, SK *C*=1) at $Ca_1 = 0.3$. (b) Trajectories of the centers of capsules for three Ca_2 at $\Delta y_{final}/a$.

Figure 9: (Color online) (a) Comparison of the variation of $D_{\max}$ with Ca_2 for pair collision of drops and capsules. Comparison of $\delta y_{final}/a$ between Drop and Capsule at two Ca_2 values.

Figure 10: Relative trajectory of a pair of capsules in homogenous collision at different *C* for Skalak model at $Ca = 0.3$, x_0/a=4 and $y_0/a = 0.5$. Inset shows the variation of $\Delta y_{final}/a$ with *C*. (b) Effect of C on the variation of $\delta y_{final}/a$ of the C_1 with Ca_2. Inset shows the plot for $D_{\max}$ of C_1 with Ca_2 at different *C*.